

pubs.acs.org/JPCL Letter

Crystal Symmetry and Static Electron Correlation Greatly Accelerate Nonradiative Dynamics in Lead Halide Perovskites

Brendan Smith, Mohammad Shakiba, and Alexey V. Akimov*



Cite This: J. Phys. Chem. Lett. 2021, 12, 2444-2453



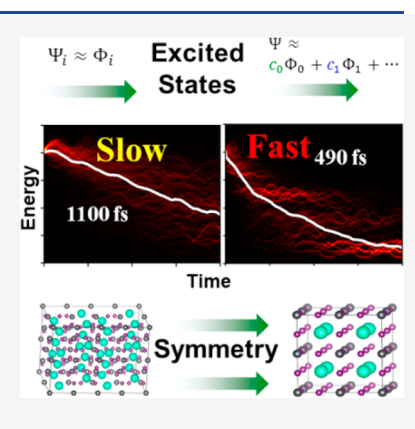
ACCESS

Metrics & More

Article Recommendations

Supporting Information

ABSTRACT: Using a recently developed many-body nonadiabatic molecular dynamics (NA-MD) framework for large condensed matter systems, we study the phonon-driven nonradiative relaxation of excess electronic excitation energy in cubic and tetragonal phases of the lead halide perovskite CsPbI₃. We find that the many-body treatment of the electronic excited states significantly changes the structure of the excited states' coupling, promotes a stronger nonadiabatic coupling of states, and ultimately accelerates the relaxation dynamics relative to the single-particle description of excited states. The acceleration of the nonadiabatic dynamics correlates with the degree of configurational mixing, which is controlled by the crystal symmetry. The higher-symmetry cubic phase of CsPbI₃ exhibits stronger configuration mixing than does the tetragonal phase and subsequently yields faster nonradiative dynamics. Overall, using a many-body treatment of excited states and accounting for decoherence dynamics are important for closing the gap between the computationally derived and experimentally measured nonradiative excitation energy relaxation rates.



Nonadiabatic (NA) molecular dynamics (MD) is a promising method for revealing mechanisms and characterizing the dynamics of NA processes. Multiple NA-MD studies of bulk perovskites have been undertaken to date, providing insight into the role of cation¹ and halide² identity, symmetry breaking at grain boundaries,³ and vacancies⁴ in determining the kinetics of such processes. Other works have reported NA-MD studies of the nonradiative hot carrier relaxation and electron—hole recombination processes in perovskite nanocrystals,⁵ 2D perovskites,^{6–8} and related heterostructure systems.^{9–11} Currently, NA-MD simulations of complex systems such as condensed phase or nanoscale materials, including lead halide perovskites (LHPs), rely on the use of a single-particle (SP) description of the electronic excited states.^{12–18} Within this description, the Coulomb and exchange interactions between electrons and holes are neglected, and the electrons and holes are considered free particles.

While the SP treatment of the electronic states has been shown to be reasonable under certain conditions, ¹⁹ it breaks down in many other cases. ^{20,21} Notably, for systems possessing symmetry, electronic state degeneracies become important, suggesting that the true excited states may be best described by the superpositions of such (nearly)-degenerate states. Under such conditions, the static electronic correlation becomes important to include, because nearly all excited states, but the lowest few, typically contain multiple SP excitations (Slater determinants). A many-body (MB) description of the excited electronic states is also necessary in quantum-confined systems ^{22–25} and at low temperatures, ^{26,27} where exciton

formation may be strongly favored. Furthermore, modeling processes that involve excited states' interaction, such as triplet—triplet annihilation and photon upconversion, ^{28–31} singlet fission, ^{32–34} and excimer formation, ^{35,36} would also require stepping beyond the commonly adopted SP approximation and extending the NA methodology to the MB (multiconfigurational) treatment of the electronic states.

NA-MD calculations that utilize a high-level description of electronic excited states (naturally including MB effects) are routinely possible nowadays directly for relatively small molecular systems^{37–41} or via QM/MM approaches for larger systems. In contrast, the inclusion of MB effects in the NA-MD of nanoscale, periodic, and extended molecular systems can be prohibitively expensive. While an MB description of electronic excited states in condensed matter systems is possible, ^{42–48} such calculations are extremely expensive for their routine applications in dynamics. A number of works have reported various approaches to incorporate MB effects into the NA-MD in the past. Nakai⁴⁹ utilized the time-dependent density functional tight-binding (TD-DFTB)^{50,51} approach to model NA-MD in LHPs. Bonafe⁵² have recently developed an Ehrenfest TD-DFTB approach to modeling coupled elec-

Received: December 24, 2020 Accepted: March 1, 2021 Published: March 4, 2021





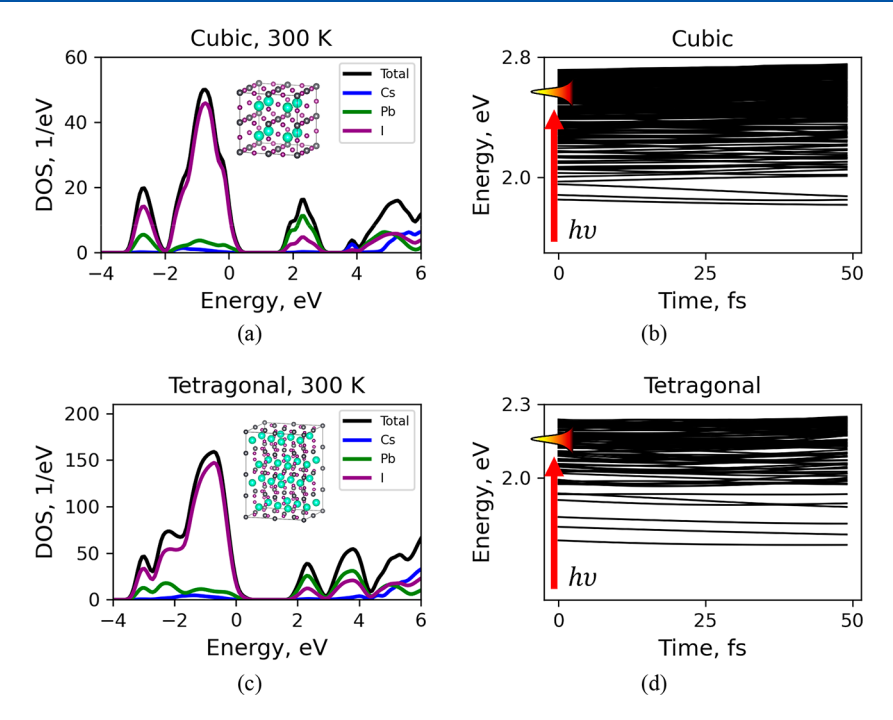


Figure 1. Thermally averaged projected density of states for the considered CsPbI₃ systems and schematics of some of the considered electronic excitations. (a) pDOS for the cubic phase; (b) schematic of electronic excitation resulting in \sim 0.8 eV of excess electronic energy for the cubic phase; (c) pDOS for the tetragonal phase; (d) schematic of electronic excitation resulting in \sim 0.4 eV of excess electronic energy for the tetragonal phase.

tron-nuclear dynamics within the DFTB+50 package and applied it to study the excited-state dynamics in several example systems. The Tretiak group has developed the NEXMD^{53,54} software package that relies on the collective electron oscillator (CEO) approach 55,56 for NA-MD modeling in extended organic systems. A number of schemes based on the TD-DFT description of electronic excited states have been reported recently⁵⁷⁻⁵⁹ as an affordable way of incorporating MB effects into NA-MD,^{60,61} including our own implementation using the neglect-of-back-reaction approximation (NBRA) of NA-MD within the Libra software. 62,63 Despite these recent advances, the use of the SP description of electronic excited states in the NA-MD of nanoscale and periodic systems is still prevailing. To date, little attention has been paid to critically assessing the approximate approaches in view of the more rigorous methods currently available. Thus, an assessment of the role of MB effects in the NA-MD of such extended systems is of high importance.

In this work, we report our studies of MB effects in the NA-MD of periodic condensed matter systems under conditions favoring high (quasi) degeneracies of the electronic states, as may be the case for LHPs. In particular, we focus on modeling excess excitation energy relaxation in the CsPbI₃ LHP, which is known to exist in the cubic and tetragonal phases (among others). Our expectation here is that the difference in symmetries of the crystal structures of the two phases can affect the degeneracies of electronic states, leading to differences in the many-body composition of the excited electronic states for the two systems. In this way, we examine the role of crystal symmetry on the NA dynamics in condensed matter systems. Furthermore, we assess the role that MB effects have in the NA-MD by studying the dynamics in these two systems at both the MB and SP levels.

We employ atomistic models of the cubic and tetragonal phases of CsPbI₃ composed as $2 \times 2 \times 2$ supercells and

containing 40 and 160 atoms, respectively (Figure 1, panels a and c, insets). The geometry optimization, molecular dynamics, ground-state density functional theory (DFT), and TD-DFT calculations are performed using the CP2K software package. 64,65 In the electronic structure calculations, the valence electrons for all atom types are described using a mixed Gaussian and plane-wave basis set. The exchange and correlation of the valence electrons is described by the Perdew-Burke-Ernzerhof (PBE)⁶⁶ density functional. Although, this pure density functional has a number of wellknown problems, ^{67–71} the use of generally more reliable hybrid functionals in the MD calculations such as those undertaken in the present work is prohibitively expensive. We anticipate that the qualitative trends discussed in this work will hold even if the hybrid functionals are used, except for the cases explicitly discussed later. The effects of the core electrons are accounted for using Goedecker-Teter-Hutter (GTH)⁷² pseudopotentials. The plane-wave basis is determined by the charge density cutoff of 300 Ry. The double-ζ-valence-polarized (DZVP) basis set⁷³ is used as the Gaussian basis. To ensure the accuracy of the force calculations, the k-point sampling uses the $4 \times 4 \times 4$ and $2 \times 2 \times 2$ Monkhorst-Pack grids⁷⁴ for the cubic and tetragonal systems, respectively. Dispersion interactions are accounted for using Grimme's DFT-D3 dispersion correction.⁷⁵ Each system is first thermalized to 300 K using MD followed by production MD. The production MD trajectories are run for 1.8 ps and are sampled using nuclear integration time steps of 1 fs. Thermal effects of the bath are described by a canonical sampling through velocity rescaling (CSVR)⁷⁶ thermostat with a time constant of 200 fs, as was used in a previous study by Uratani and Nakai, which is within the range of phonon modes for this perovskite.⁴⁹ For all geometry optimization calculations, optimization is performed using the Broyden-Fletcher-Goldfarb-Shannon (BFGS) algorithm.⁷⁷ The geometry optimization process is continued

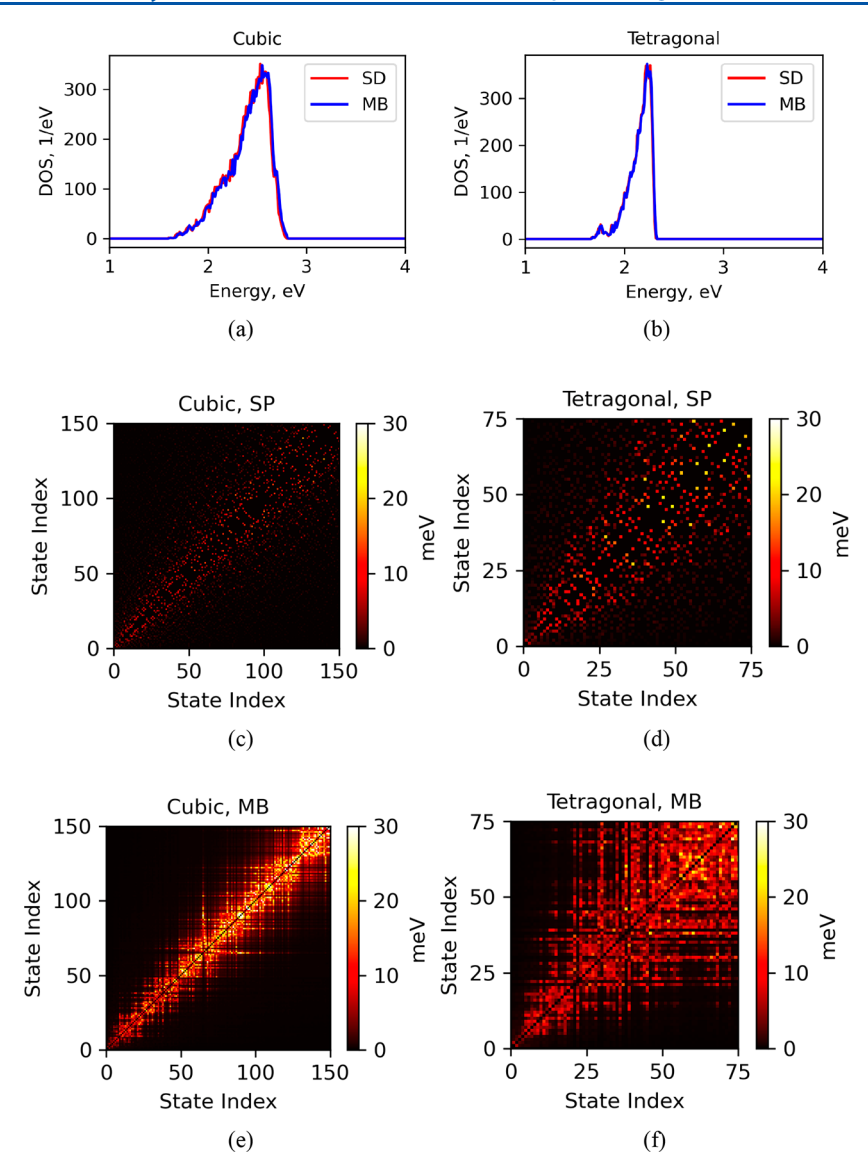


Figure 2. Comparison of densities of excited states and thermally averaged nonadiabatic couplings for the cubic (a, c, and e) and tetragonal (b, d, and f) phases of CsPbI₃. The thermally averaged NACs are computed at the SP (c and d) and MB (e and f) levels.

for each structure until the maximum force on each atom becomes less than 15 meV/Å and the maximum geometry change becomes less than 0.002 Bohr.

For both systems, the thermally averaged electronic band gaps are roughly 1.8 eV (Figure 1), which is in good agreement with experiments. 78,79 Thermal averaging is done over all the configurations sampled by the MD trajectories. We find that averaging yields a converged pDOS (Figure S1). Considering the level of electronic structure calculations used in this work, such a good agreement of the band gap values for these LHPs likely stems from the known error cancellation that occurs when using pure functionals without spin-orbit coupling (SOC) effects. The projected density of states (pDOS) calculations reveal that for both systems, the valence bands are primarily composed of atomic orbitals of the iodine atoms, whereas the conduction bands are composed primarily of lead orbitals with a smaller fraction of iodine orbitals (Figure 1), in agreement with previous theoretical works. 80,81 The main differences between the cubic and tetragonal phases is the increased pDOS in the latter, which is a consequence of a larger size of the cell. Thus, one may expect faster relaxation of excess electronic energy in the tetragonal phase. In addition, the tetragonal system has two groups of conduction band states in the energy window 2–4 eV, whereas the cubic has only one. The group of states near 2 eV is split into 3 substates in the cubic system in the static structure (Figure S1), but this fine structure is hidden in the thermally averaged pDOS (Figure 1). The two bands of the tetragonal system do not show any notable fine structure in the static calculations. The pDOS structure can be rationalized by the system symmetries: the 3-fold splitting of a single band in the cubic structure can be attributed to the 3-fold symmetry of the system, whereas the presence of the two notably split bands in the tetragonal system can be attributed to a notable anisotropy of its crystal structure, with at least 2 distinct directions (e.g., c vs a or b).

We compare properties relevant for NA-MD calculations computed at the SP and MB levels (Figure 2). As was shown earlier, ^{82,83} NACs between distinct Slater determinants (SDs) can be reduced to the NACs between orbitals. For this reason, the basis of single SD excitations is considered a SP description. In contrast, the MB electronic states are described by superpositions of the SD excitations. Because the densities

of excited states are rather high, we considered only finite energy windows of excited states to compute: roughly 0.9 eV for the cubic and 0.5 eV for the tetragonal phases. At the MB level, 151 and 76 excited states fit into these energy spans for the cubic and tetragonal phases, respectively. These MB states are formed in the basis of 229 and 118 unique SDs for the cubic and tetragonal systems, respectively. However, some of these excitations are outside of the energy windows considered and therefore may be excluded from the SP-only modeling and calculations. Following the earlier approximation some of the SP excited states are estimated via the differences of orbital energies, neglecting the Coulomb and exchange integrals.

Somewhat surprisingly, the densities of the excited states computed at both SP and MB levels for each system are nearly the same (Figure 2, panels a and b). This similarity indicates that the excitonic effects (static correlation and Coulombic interaction of electron-hole pairs) are relatively small. This result is consistent with experimental studies reporting small exciton binding energies in LHPs. 94,95 Small excitonic effects in the presently studied systems are also expected because of the lack of quantum confinement on one hand and the use of a pure density functional on the other. As suggested by Izmaylov and Scuseria,⁹⁶ and as also follows from other studies,⁹ capturing excitonic effects in TD-DFT calculations requires the functional with the correct asymptotic behavior of the exchange, such as achieved via the use of hybrid functionals, especially the long-range corrected ones. However, such calculations are prohibitively expensive, and we leave this question an open problem.

Given the similarity of the DOS in the MB and SP bases, one may expect that the NACs in the MB and SP excitation bases would be comparable. However, a detailed analysis of the NACs between the pairs of MB and SP states breaks this expectation. The first distinction comes in the structure of the NAC matrices. At the SP excitation level, the time-averaged NACs between electronic states have a scattered-like appearance (Figure 2, panels c and d). Such a structure arises because in the space of SP states of type HOMO- $N \rightarrow$ LUMO+M, with varying N and M, and ordered by energy, the corresponding SDs may differ by more than one electron excitation, leading to zero coupling between such pairs of states. On the other hand, the MB electronic excited states are composed of multiple SP transitions, and two MB states may become coupled via the coupling of the underlying SDs. As a result, the NAC matrix has a more "filled-in" structure when computed in the basis of MB excited states (Figure 2, panels e and f). Furthermore, we find that the probability distributions of the NACs between MB states is shifted toward larger values compared to the probability distributions of the NACs between SP states (Figure S2). This means that one is more likely to encounter larger magnitudes of NACs during the course of the dynamics if MB effects are accounted for. The probability to find near-zero NACs is higher at the SP level than at the MB level. For both cubic and tetragonal phases, the probability to find NAC values greater than ca. 0.2 meV in absolute value is larger in the MB basis than the SP basis (Figure S2, panels a and d). The probability of finding NACs with the absolute values of 5-50 meV is small for both systems, which is orders of magnitude smaller than to encounter NACs in the range 0-0.5 meV. However, for all values of NAC magnitudes, the probability density is consistently larger at the MB level that it is at the SP level.

Taken together, we expect that both the shift of the NAC probability density toward larger values and the changed structure of the NAC matrix should accelerate the excited-state dynamics (e.g., excited-state relaxation) when computed at the MB level relative to dynamics at the SP level.

It is illustrative to discuss the origin of the difference in the NAC magnitudes computed at the SP and MB levels. At every time instant, the MB states, $\{\Psi_i\}$, are given by a unitary transformation (U) of the SP excitations, $\{\Phi_i\}$: $\Psi_i = \sum_i U_{ii} \Phi_i$. The NACs between the MB states are given by d_{ij}^{MB} = $\left\langle \Psi_{i} \left| \frac{\partial}{\partial t} \right| \Psi_{j} \right\rangle = \sum_{a,b} U_{ia}^{*} U_{bj} \left\langle \Phi_{a} \left| \frac{\partial}{\partial t} \right| \Phi_{b} \right\rangle + \sum_{a,b} U_{ia}^{*} \langle \Phi_{a} | \Phi_{b} \rangle \frac{\partial}{\partial t} U_{bj} = 0$ $\sum_{a,b}U_{ia}^*d_{ab}^{\mathrm{SP}}U_{bj}+\sum_aU_{ia}^*rac{\partial}{\partial t}U_{aj}.$ Here, we utilized the orthonormalization of the SP states, $\langle \Phi_i | \Phi_j \rangle = \delta_{ij}$. Under the special case of the time-independent transformation matrix U, $\frac{\partial}{\partial t}U=0$, one can show that the average magnitude of the NACs in the two bases are equal, as for instance could be quantified by $\sum_{ij} |d_{ij}|^2$. Using the fact that the matrix U is a unitary transformation, one can show that $\sum_{i,j \in \{MB\}} |d_{ij}|^2 = \sum_{i,j \in \{SP\}} |d_{ij}|^2$. Thus, the average magnitude of the coupling would not depend on whether the SP or MB description of excited states is used. However, in most situations, the transformation matrix U is time-dependent, because of the time-dependence of the Hamiltonian via its parametric dependence on nuclear trajectories. As such, the term $\sum_a U_{ia}^* \frac{\partial}{\partial t} U_{aj}$ can not be neglected. It is this term that is responsible for the difference in the average NAC magnitudes (as quantified by the centers of gravity in the probability density distributions shown in Figure S2). In other words, the time-dependence of the MB states composition in terms of the corresponding SP states determines the difference in average NACs. Having said that, even the condition $\sum_{i,j\in\{\mathrm{MB}\}} |d_{ij}|^2 = \sum_{i,j\in\{\mathrm{SP}\}} |d_{ij}|^2 \text{ does not imply a similarity of}$ the dynamics computed in the two bases. The relative magnitude of the couplings between "equivalent" states (if such a mapping of the SP to MB basis can be made) may be changed, such that some channels of the dynamics may be favored in one basis over the other. Finally, although our current calculations suggest faster dynamics in the MB basis, there is no reason to expect this to be a general trend. In principle, there is no limitation for the term $\sum_a U_{ia}^* \frac{\partial}{\partial t} U_{aj}$ to take values opposite in sign to those of the $\sum_{a,b} U_{ia}^* d_{ab}^{SP} U_{bj}$ term, thus decreasing the effective NACs in the MB basis as opposed to those in the SP basis.

Comparing the crystal symmetries, we find that NACs are larger in the cubic system than in the tetragonal one (Figures 2 and S2). This difference can be rationalized by the larger degree of configurational mixing in the cubic system. We quantify the degree of configurational mixing by the squared amplitudes of the configuration interaction coefficients of dominant SDs entering the composition of the MB states (Figures S3 and S4). Our analysis shows that the first few excited states are mainly SP in both systems at their optimized geometries, which validates the widely used SP approximation in modeling NA processes such as electron-hole recombination. 85,98,99 In the tetragonal system, electronic states retain a strong SP character for many of the low-lying electronic states (Figures S4), whereas in the cubic system, all but the lowest excited states exhibit significant configurational mixing (Figure S3). We attribute such a pronounced mixing of the SP states to

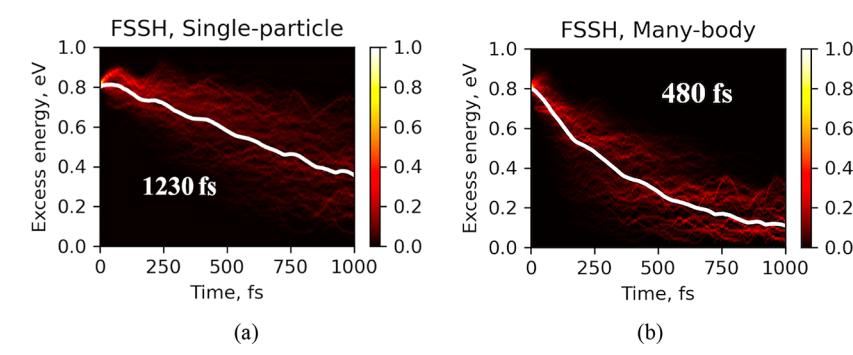


Figure 3. Excess electronic energy relaxation dynamics computed with the FSSH methodology in cubic CsPbI₃: (a) at the SP level and (b) at the MB level.

the increased symmetry present in the cubic system. High symmetry leads to high degeneracy of electronic states in the space of SP transitions and promotes their mixing in the MB picture. At lower temperatures, when thermally induced atomic motion is reduced, the symmetry of the crystal structure is better preserved. This explains the stronger configurational mixing present at the optimized geometries (0 K, Figure S3, panels a and b; Figure S4, panels a and b) compared to the thermally sampled set of configurations at 300 K (Figure S3, panels c and d; Figure S4, panels c and d). At 300 K, the atomic motion breaks the symmetry and reduces the degree of configurational mixing. However, the influence of the systems' symmetry is still present. For the cubic system, significant configurational mixing of the electronic states is still present at 300 K, especially for higher-energy excitations.

To directly assess the role of MB effects on the NA dynamics, we conduct explicit NA-MD calculations using the fewest switches surface hopping (FSSH), ¹⁰⁰ Belyaev–Lebedev–Landau–Zener (BLLZ), ^{101,102} and several decoherence correction methodologies, ^{103–105} as also detailed in the section 4 of the Supporting Information. We employ a recently developed interface of the Libra software for NA-MD calculations ^{62,63} and the CP2K⁶⁴ code. The details of our computational setups are summarized in section 5 of the Supporting Information. Further details of our NA-MD framework are discussed elsewhere. ¹⁰⁶ The dynamics of excess electronic excitation energy relaxation for the considered systems is quantified by fitting the average excess electronic excitation energy relaxation dynamics over all NA-MD trajectories to the following functional form:

$$f(t; E_0) = A \exp\left(-\left(\frac{t}{\tau_1}\right)\right) + (E_0 - A) \exp\left(-\left(\frac{t}{\tau_2}\right)^2\right) \tag{1}$$

Such a fitting function has been used in past NA-MD studies to characterize the decay of excess excitation energy in condensed matter and nanoscale systems. This form accounts for the Gaussian decay kinetics typical for coherent dynamics of electrons in dense manifolds of excited states in the short-time range and the exponential decay kinetics typical for incoherent dynamics at the longer time scales or in the sparse manifolds of excited states. The overall relaxation time scale is then computed according to

$$\tau = \frac{A}{E_0}\tau_1 + \frac{(E_0 - A)}{E_0}\tau_2 \tag{2}$$

The MB effects on the NA dynamics can be best seen by comparing the excitation energy excess decay kinetics at the FSSH level for both systems. When MB effects are accounted for, the relaxation of excess excitation energy is accelerated by the factor of 2.6 (Figure 3). Moreover, the inclusion of MB effects qualitatively changes the dynamics. At the MB level, it is typically the case that the exponential component in eq 1 is smaller than it is in the SP basis (e.g., see Table S1 of the Supporting Information), which signifies that coherent dynamics is prominent in the MB basis. The coherent dynamics in the MB basis is favored by the more extensive coupling of all states to each other as compared to the SP picture. At the SP level, the dynamics exhibits little to no decay for the first 100 fs and is followed by a slow decay (Figure 3a). In the SP basis, the decay kinetics is dominated by the exponential component in eq 1 (e.g., see Table S1 of the Supporting Information), which signifies that the coherent dynamics is suppressed or intrinsically slower in the SP basis. This suppression of the coherent dynamics can be explained by larger energy gaps between the coupled states. In this regard, one should not be mislead by the apparently similar densities of excited states in the SP and MB bases (Figure 2, panels a and b). Although the densities are similar, they do not reflect the structure of the coupling of the states—the energetically nearby SP states may be uncoupled, whereas the average energy gaps between the coupled states would be larger in this basis.

We compute the time scales of excess excitation energy decay in both cubic and tetragonal phases of CsPbI₃ using both the SP and MB description of excited states and several NA-MD methodologies (Table 1, also see section 6 of the Supporting Information for more details). Our main observation is that the dynamics with the MB effects accounted for is generally faster than it is in the basis of SP states. This conclusion is consistent with the changes of the NAC matrix structure discussed above. The inclusion of the MB effects accelerates the dynamics more in the cubic system than it does in the tetragonal system: the time scales are decreased by the factor of 1.4-2.6 in the cubic system and by a factor of only 1.6 in the tetragonal one in comparison to the corresponding SP-based time scales. Such trends are also consistent with slightly larger NACs in the cubic system than in the tetragonal, as a consequence of the crystal symmetries (e.g., see Figures

As expected, accounting for electronic decoherence (via ${\rm ID-A^{104}}$ and ${\rm mSDM^{103,105}}$ methods) leads to slowing the dynamics down relative to FSSH. Of the two decoherence-corrected TSH schemes tested, the ID-A typically yields a

Table 1. Excited-State Energy Decay Time Constants, τ (fs), Computed Using Various Surface Hopping Methods at Either the SP or MB Description of the Electronic Excited States^a

experiment, 1. 4 eV, 0.8 eV		476, Bretschneider et al., ¹⁰⁸ ~1000 Shen et al. ¹⁰⁹ , ¹¹⁰			
cubic		FSSH	ID-A	mSDM	BLLZ
MB	0.8 eV	480	1209	1187	486
SP	0.8 eV	1226	1757	2492	444
MB	0.4 eV	679	1120	1645	984
SP	0.4 eV	1116	1323	1858	889
tetragonal		FSSH	ID-A	mSDM	BLLZ
MB	0.4 eV	1002	1617	1823	1865
SP	0.4 eV	1655	2424	3090	1843

 $^{a}E_{0}$ (eV) is the initial excess electronic excitation energy used in the calculation setup and the fitting function, eq 1.

faster dynamics than mSDM. In contrast to all the NAC-based TSH methods used (FSSH, ID-A, and mSDM), the energybased BLLZ method predicts highly similar dynamics of the excited states at both the MB and SP levels. MB effects can influence the dynamics in two ways. One is via the wave functions (and hence the NACs), via the mixing of excited SDs, as discussed above, which we refer to as weak excitonic effects. The other is via the energies of the excitonic states, which we refer to as strong excitonic effects. As discussed previously, the strong excitonic effects would manifest themselves in quantum-confined systems and require the use of density functionals with the proper asymptotic behavior of the exchange terms ⁹⁷ (pragmatically speaking, the use of rangecorrected hybrid functionals). In other words, the strong excitonic effects would manifest themselves via a notable exciton binding energy. For the systems considered in this work, the densities of the MB and SP excited states agree with each other (Figure 2, panels a and b), suggesting the exciton binding energies are small and the SP picture works as far as the energies of the electronic excited states are concerned. This observation agrees with the 10 meV value for cubic CsPbI₃ reported by the prior studies. 94,95 This energy is smaller than thermal energy at room temperature, so the excitonic effects are negligible. The similarity of the densities of excited states at the SP and MB levels explains the insensitivity of the energybased BLLZ to the level of the description of excited-state energies. This behavior may be regarded as a consequence of the lack of strong excitonic effects or inability to capture it, which can be a consequence of the lack of quantum confinement (3D systems) and the use of pure density functional. With the "strong excitonic effects" ruled out in the present study, we conclude that acceleration of the NA-MD we observe in periodic LHPs can be attributed to the "weak" excitonic effects, that is, the mixing of the quasi-degenerate states, which in turn can be affected by a system's symmetry.

We anticipate though that applying the current approach to 2D or 0D perovskites/systems and/or using hybrid functionals (which is prohibitively expensive at this point) may change the computed time scales and the qualitative comparison of the time scales computed with the BLLZ approach. In this regard, recent work by Liu et al.⁶⁰ demonstrated that accounting for strong excitonic effects in quantum-confined systems like the MoS₂/WS₂ heterojunction may lead to up to a 10-fold acceleration of the dynamics compared to the commonly used SP Kohn–Sham-DFT prescription of excited states. Such an

acceleration is notably larger than the approximately 2.6-fold acceleration because of weak excitonic effects seen in the present work, although the two values cannot be compared directly as they are obtained for distinct systems.

An analysis of Table 1 shows that the computed energy relaxation time scales may be in a good agreement with the reported experimental data depending on the combination of the excited states' description level and the TSH methodology used. Such agreements and disagreements should be taken critically because they may be due to fortuitous error cancellations or the lack of known effects that are too expensive to include, respectively. At the MB level, the FSSH calculations for the cubic system are in excellent agreement with the experimental time scales of approximately 476 fs of Bretschneider et al. 108 At the SP level, the computed time scales are nearly twice as slow: 1.1-1.2 ps for a range of initial excitation energy levels. These time scales are consistent with the values reported in a previous computational study that relied on a similar SP description of excited states. In contrast, Shen et al. 109,110 report time scales in the range of 1-30 ps depending on the carrier density, with a subpicosecond (0.8-1.0 ps) range for low carrier densities studied in their experiment. One may think that the FSSH at the SP level yields a reasonable agreement with the experiment. However, the FSSH does not account for decoherence effects present in realistic systems. Thus, one needs to shift attention to the ID-A and mSDM results. At the MB level, the dynamics computed using these schemes comes into closer agreement with the ca. 1 ps time scales of Shen et al. 109,110 The SP description would overestimate the time scales by approximately a factor of 2 compared to the data of Shen et al. and by a factor of 4-5 compared to the data of Bretschneider et al. Thus, the inclusion of even weak excitonic effects is critical for merging the gap between computed and experimentally measured time scales of excitation energy relaxation.

The above discussion should be taken critically. Our simulations do not explicitly include SOC effects, which have been shown to significantly accelerate dynamics in LHPs. 111 At the same time, we use a pure density functional instead of the computationally more expensive hybrid functionals, and it has been demonstrated before that the use of hybrid functionals may slow down the dynamics. 18 It is possible that the two approximations may counter each other's effect, although we cannot tell to what extent. Nonetheless, as shown in this work, weak excitonic effects may lead to a notable acceleration of the dynamics. This effect is likely to hold regardless of what functional is used and whether the SOC effects are included, although further studies on this matter would be highly desirable.

Another potential limitation of the current methodology, as well as of other similar techniques, concerns the treatment of electron and phonon k-points. On one hand, including a larger number of k-points (or, equivalently, using a larger supercell) could increase the density of electronic states and accelerate the decay dynamics. On the other hand, describing the transitions between the k-points requires accounting for phonon quantization (q-points), which would require a different computational methodology that is not available in the current scheme. Such calculations may also involve an extremely large number of k-points, 112 which is prohibitively expensive for the atomistic systems considered here (especially at the TD-DFT level). At the same time, enabling relaxation channels that include multiple k-points may slow the decay

dynamics, because a fraction of the relaxation will take place across different k-points or at k-points other than the Γ -point. In our experience, NACs are larger for the k-points closer to the Γ -point and are smaller across the k-points, at least for direct gap semiconductors. Thus, on average, enabling relaxation dynamics across multiple k-point states may lead to a slower average decay of the excited states, which may counter the effect of the increased densities of states. Overall, the inclusion of multiple k-points may or may not be another factor to lower the gap between the computationally derived carrier relaxation times (on the higher end) and the experimentally determined ones (on the smaller end). For both outcomes, however, MB effects are expected to accelerate the dynamics of the excited-state relaxation, whether it brings the computed results closer to or farther away from the experimental references.

In summary, we show that including MB effects in NA-MD simulations may greatly accelerate the nonradiative relaxation of excess electronic excitation energy. We demonstrate that for the CsPbI₃ perovskite, this acceleration factor reaches a value of 2.6 but nonetheless is sufficient to bring the computed NA-MD time scales into a closer agreement with experiments. The nonadiabatic excess electronic excitation energy relaxation rates are larger in systems with high symmetry, such as in the cubic phase of CsPbI₃, as compared to the lower-symmetry, tetragonal phase. High spatial symmetry facilitates the mixing of multiple excited SDs comprising the excited states, leads to an increased coupling between the excited states, and leads to faster NA-MD.

ASSOCIATED CONTENT

Supporting Information

The Supporting Information is available free of charge at https://pubs.acs.org/doi/10.1021/acs.jpclett.0c03799.

(1) pDOS at the optimized geometries, (2) comparison of the NAC probability distributions, (3) analysis of the degree of configurational mixing in the many-body excited states, (4) nonadiabatic molecular dynamics methodology, (5) computational details for the NAMD, and (6) details of the excess excitation energy decay fitting functions (PDF)

AUTHOR INFORMATION

Corresponding Author

Alexey V. Akimov — Department of Chemistry, University at Buffalo, The State University of New York, Buffalo, New York 14260, United States; Occid.org/0000-0002-7815-3731; Email: alexeyak@buffalo.edu

Authors

Brendan Smith — Department of Chemistry, University at Buffalo, The State University of New York, Buffalo, New York 14260, United States; Occid.org/0000-0003-3460-9984

Mohammad Shakiba — Department of Materials Science and Engineering, Shahid Bahonar University of Kerman, Kerman, Iran

Complete contact information is available at: https://pubs.acs.org/10.1021/acs.jpclett.0c03799

Author Contributions

§B.S. and M.S. contributed equally to this work.

Notes

The authors declare no competing financial interest. Detailed scripts and input files used for all types of calculations are available in digital form online from the Zenodo server.¹¹³

ACKNOWLEDGMENTS

A.V.A. acknowledges the financial support of the National Science Foundation (Grant OAC-NSF-1931366). Support of computations is provided by the Center for Computational Research at the University at Buffalo.

REFERENCES

- (1) Madjet, M. E.; Berdiyorov, G. R.; El-Mellouhi, F.; Alharbi, F. H.; Akimov, A. V.; Kais, S. Cation Effect on Hot Carrier Cooling in Halide Perovskite Materials. *J. Phys. Chem. Lett.* **2017**, *8*, 4439–4445.
- (2) He, J.; Vasenko, A. S.; Long, R.; Prezhdo, O. V. Halide Composition Controls Electron—Hole Recombination in Cesium—Lead Halide Perovskite Quantum Dots: A Time Domain Ab Initio Study. J. Phys. Chem. Lett. 2018, 9, 1872—1879.
- (3) Wang, Y.; Fang, W.-H.; Long, R.; Prezhdo, O. V. Symmetry Breaking at MAPbI₃ Perovskite Grain Boundaries Suppresses Charge Recombination: Time-Domain Ab Initio Analysis. *J. Phys. Chem. Lett.* **2019**, *10*, 1617–1623.
- (4) He, J.; Long, R. Lead Vacancy Can Explain the Suppressed Nonradiative Electron—Hole Recombination in FAPbI₃ Perovskite under Iodine-Rich Conditions: A Time-Domain Ab Initio Study. *J. Phys. Chem. Lett.* **2018**, *9*, 6489—6495.
- (5) Boehme, S. C.; Brinck, S. ten; Maes, J.; Yazdani, N.; Zapata, F.; Chen, K.; Wood, V.; Hodgkiss, J. M.; Hens, Z.; Geiregat, P.; et al. Phonon-Mediated and Weakly Size-Dependent Electron and Hole Cooling in CsPbBr₃ Nanocrystals Revealed by Atomistic Simulations and Ultrafast Spectroscopy. *Nano Lett.* **2020**, *20*, 1819–1829.
- (6) Zhang, Z.; Fang, W.-H.; Long, R.; Prezhdo, O. V. Exciton Dissociation and Suppressed Charge Recombination at 2D Perovskite Edges: Key Roles of Unsaturated Halide Bonds and Thermal Disorder. J. Am. Chem. Soc. 2019, 141, 15557–15566.
- (7) Zhang, S.-F.; Chen, X.-K.; Ren, A.-M.; Li, H.; Bredas, J.-L. Impact of Organic Spacers on the Carrier Dynamics in 2D Hybrid Lead-Halide Perovskites. *ACS Energy Lett.* **2019**, *4*, 17–25.
- (8) He, J.; Fang, W.-H.; Long, R. Two-Dimensional Perovskite Capping Layer Simultaneously Improves the Charge Carriers' Lifetime and Stability of MAPbI₃ Perovskite: A Time-Domain Ab Initio Study. *J. Phys. Chem. Lett.* **2020**, *11*, 5100–5107.
- (9) Long, R.; Prezhdo, O. V. Dopants Control Electron—Hole Recombination at Perovskite—TiO₂ Interfaces: Ab Initio Time-Domain Study. *ACS Nano* **2015**, *9*, 11143—11155.
- (10) Zhang, J.; Hong, H.; Zhang, J.; Fu, H.; You, P.; Lischner, J.; Liu, K.; Kaxiras, E.; Meng, S. New Pathway for Hot Electron Relaxation in Two-Dimensional Heterostructures. *Nano Lett.* **2018**, *18*, 6057–6063.
- (11) Long, R.; Fang, W.-H.; Prezhdo, O. V. Strong Interaction at the Perovskite/ ${\rm TiO_2}$ Interface Facilitates Ultrafast Photoinduced Charge Separation: A Nonadiabatic Molecular Dynamics Study. *J. Phys. Chem.* C **2017**, *121*, 3797–3806.
- (12) He, J.; Fang, W.-H.; Long, R.; Prezhdo, O. V. Why Oxygen Increases Carrier Lifetimes but Accelerates Degradation of CH₃NH₃PbI₃ under Light Irradiation: Time-Domain Ab Initio Analysis. *J. Am. Chem. Soc.* **2020**, *142*, 14664–14673.
- (13) Banerjee, S.; Kang, J.; Zhang, X.; Wang, L.-W. The Effects of Interstitial Iodine in Hybrid Perovskite Hot Carrier Cooling: A Non-Adiabatic Molecular Dynamics Study. *J. Chem. Phys.* **2020**, *152*, 091102.
- (14) Carof, A.; Giannini, S.; Blumberger, J. How to Calculate Charge Mobility in Molecular Materials from Surface Hopping Non-Adiabatic Molecular Dynamics—beyond the Hopping/Band Paradigm. *Phys. Chem. Chem. Phys.* **2019**, *21*, 26368–26386.
- (15) Oliboni, Ř. S.; Yan, H.; Fan, H.; Abraham, B.; Avenoso, J. P.; Galoppini, E.; Batista, V. S.; Gundlach, L.; Rego, L. G. C. Vibronic

- Effects in the Ultrafast Interfacial Electron Transfer of Perylene-Sensitized TiO₂ Surfaces. J. Phys. Chem. C 2019, 123, 12599-12607.
- (16) Ziogos, O. G.; Giannini, S.; Ellis, M.; Blumberger, J. Identifying High-Mobility Tetracene Derivatives Using a Non-Adiabatic Molecular Dynamics Approach. *J. Mater. Chem. C* **2020**, *8*, 1054–1064.
- (17) Agrawal, S.; Lin, W.; Prezhdo, O. V.; Trivedi, D. J. Ab Initio Quantum Dynamics of Charge Carriers in Graphitic Carbon Nitride Nanosheets. J. Chem. Phys. 2020, 153, 054701.
- (18) Candiotto, G.; Torres, A.; Mazon, K. T.; Rego, L. G. C. Charge Generation in Organic Solar Cells: Interplay of Quantum Dynamics, Decoherence, and Recombination. *J. Phys. Chem. C* **2017**, *121*, 23276–23286.
- (19) Fischer, S. A.; Habenicht, B. F.; Madrid, A. B.; Duncan, W. R.; Prezhdo, O. V. Regarding the Validity of the Time-Dependent Kohn—Sham Approach for Electron-Nuclear Dynamics via Trajectory Surface Hopping. *J. Chem. Phys.* **2011**, *134*, 024102.
- (20) Barbatti, M.; Crespo-Otero, R. Surface Hopping Dynamics with DFT Excited States. *Top. Curr. Chem.* **2014**, *368*, 415–444.
- (21) Maitra, N. T. On Correlated Electron-Nuclear Dynamics Using Time-Dependent Density Functional Theory. *J. Chem. Phys.* **2006**, 125, 014110.
- (22) Wang, H.; Liu, W.; He, X.; Zhang, P.; Zhang, X.; Xie, Y. An Excitonic Perspective on Low-Dimensional Semiconductors for Photocatalysis. *J. Am. Chem. Soc.* **2020**, *142*, 14007–14022.
- (23) Blancon, J.-C.; Stier, A. V.; Tsai, H.; Nie, W.; Stoumpos, C. C.; Traoré, B.; Pedesseau, L.; Kepenekian, M.; Katsutani, F.; Noe, G. T.; et al. Scaling Law for Excitons in 2D Perovskite Quantum Wells. *Nat. Commun.* **2018**, *9*, 2254.
- (24) Li, Y.; Shu, H.; Wang, S.; Wang, J. Electronic and Optical Properties of Graphene Quantum Dots: The Role of Many-Body Effects. *J. Phys. Chem. C* **2015**, *119*, 4983–4989.
- (25) Hong, X.; Ishihara, T.; Nurmikko, A. V. Dielectric Confinement Effect on Excitons in PbI₄-Based Layered Semiconductors. *Phys. Rev. B: Condens. Matter Mater. Phys.* **1992**, *45*, 6961–6964.
- (26) Milot, R. L.; Eperon, G. E.; Snaith, H. J.; Johnston, M. B.; Herz, L. M. Temperature-Dependent Charge-Carrier Dynamics in CH₃NH₃PbI₃ Perovskite Thin Films. *Adv. Funct. Mater.* **2015**, 25, 6218–6227.
- (27) Wehrenfennig, C.; Liu, M.; Snaith, H. J.; Johnston, M. B.; Herz, L. M. Charge Carrier Recombination Channels in the Low-Temperature Phase of Organic-Inorganic Lead Halide Perovskite Thin Films. *APL Mater.* **2014**, *2*, 081513.
- (28) Luo, X.; Liang, G.; Han, Y.; Li, Y.; Ding, T.; He, S.; Liu, X.; Wu, K. Triplet Energy Transfer from Perovskite Nanocrystals Mediated by Electron Transfer. *J. Am. Chem. Soc.* **2020**, *142*, 11270–11278.
- (29) Luo, X.; Han, Y.; Chen, Z.; Li, Y.; Liang, G.; Liu, X.; Ding, T.; Nie, C.; Wang, M.; Castellano, F. N.; et al. Mechanisms of Triplet Energy Transfer across the Inorganic Nanocrystal/Organic Molecule Interface. *Nat. Commun.* **2020**, *11*, 28.
- (30) Wieghold, S.; Nienhaus, L. Precharging Photon Upconversion: Interfacial Interactions in Solution-Processed Perovskite Upconversion Devices. *J. Phys. Chem. Lett.* **2020**, *11*, 601–607.
- (31) Kafle, T. R.; Kattel, B.; Yao, P.; Zereshki, P.; Zhao, H.; Chan, W.-L. Effect of the Interfacial Energy Landscape on Photoinduced Charge Generation at the ZnPc/MoS₂ Interface. *J. Am. Chem. Soc.* **2019**, *141*, 11328–11336.
- (32) Miyata, K.; Conrad-Burton, F. S.; Geyer, F. L.; Zhu, X.-Y. Triplet Pair States in Singlet Fission. *Chem. Rev.* **2019**, *119*, 4261–4292.
- (33) Breen, I.; Tempelaar, R.; Bizimana, L. A.; Kloss, B.; Reichman, D. R.; Turner, D. B. Triplet Separation Drives Singlet Fission after Femtosecond Correlated Triplet Pair Production in Rubrene. *J. Am. Chem. Soc.* **2017**, *139*, 11745–11751.
- (34) Akimov, A. V.; Prezhdo, O. V. Nonadiabatic Dynamics of Charge Transfer and Singlet Fission at the Pentacene/C₆₀ Interface. *J. Am. Chem. Soc.* **2014**, *136*, 1599–1608.
- (35) Tian, Y.; Li, Y.; Chen, B.; Lai, R.; He, S.; Luo, X.; Han, Y.; Wei, Y.; Wu, K. Sensitized Molecular Triplet and Triplet Excimer Emission

- in Two-Dimensional Hybrid Perovskites. *J. Phys. Chem. Lett.* **2020**, *11*, 2247–2255.
- (36) Banerjee, T.; Hill, S. P.; Hermosilla-Palacios, M. A.; Piercy, B. D.; Haney, J.; Casale, B.; DePrince, A. E., III; Losego, M. D.; Kleiman, V. D.; Hanson, K. Diphenylisobenzofuran Bound to Nanocrystalline Metal Oxides: Excimer Formation, Singlet Fission, Electron Injection, and Low Energy Sensitization. *J. Phys. Chem. C* **2018**, *122*, 28478–28490.
- (37) Chakraborty, P.; Liu, Y.; Weinacht, T.; Matsika, S. Excited State Dynamics of *Cis*, *Cis* –1,3-Cyclooctadiene: Non-Adiabatic Trajectory Surface Hopping. *J. Chem. Phys.* **2020**, *152*, 174302.
- (38) Heindl, M.; González, L. A XMS-CASPT2 Non-Adiabatic Dynamics Study on Pyrrole. *Comput. Theor. Chem.* **2019**, *1155*, 38–46.
- (39) Polyak, I.; Hutton, L.; Crespo-Otero, R.; Barbatti, M.; Knowles, P. J. Ultrafast Photoinduced Dynamics of 1,3-Cyclohexadiene Using XMS-CASPT2 Surface Hopping. *J. Chem. Theory Comput.* **2019**, *15*, 3929—3940.
- (40) Peng, W.-T.; Fales, B. S.; Levine, B. G. Simulating Electron Dynamics of Complex Molecules with Time-Dependent Complete Active Space Configuration Interaction. *J. Chem. Theory Comput.* **2018**, *14*, 4129–4138.
- (41) Park, J. W.; Shiozaki, T. On-the-Fly CASPT2 Surface-Hopping Dynamics. *J. Chem. Theory Comput.* **2017**, *13*, 3676–3683.
- (42) Lewis, D. K.; Ramasubramaniam, A.; Sharifzadeh, S. Tuned and Screened Range-Separated Hybrid Density Functional Theory for Describing Electronic and Optical Properties of Defective Gallium Nitride. *Phys. Rev. Mater.* **2020**, *4*, 063803.
- (43) Lewis, D. K.; Sharifzadeh, S. Defect-Induced Exciton Localization in Bulk Gallium Nitride from Many-Body Perturbation Theory. *Phys. Rev. Mater.* **2019**, *3*, 114601.
- (44) Wu, Y.; Xia, W.; Zhang, Y.; Zhu, W.; Zhang, W.; Zhang, P. Remarkable Band-Gap Renormalization via Dimensionality of the Layered Material C_3B . *Phys. Rev. Appl.* **2020**, *14*, 014073.
- (45) Zhang, Y.; Xia, W.; Wu, Y.; Zhang, P. Prediction of MXene Based 2D Tunable Band Gap Semiconductors: GW Quasiparticle Calculations. *Nanoscale* **2019**, *11*, 3993–4000.
- (46) Iskakov, S.; Yeh, C.-N.; Gull, E.; Zgid, D. Ab-Initio Self-Energy Embedding for the Photoemission Spectra of NiO and MnO. *Phys. Rev. B: Condens. Matter Mater. Phys.* **2020**, *102*, 085105.
- (47) Wilhelm, J.; Golze, D.; Talirz, L.; Hutter, J.; Pignedoli, C. A. Toward *GW* Calculations on Thousands of Atoms. *J. Phys. Chem. Lett.* **2018**, *9*, 306–312.
- (48) Wilhelm, J.; Del Ben, M.; Hutter, J. GW in the Gaussian and Plane Waves Scheme with Application to Linear Acenes. J. Chem. Theory Comput. 2016, 12, 3623–3635.
- (49) Uratani, H.; Nakai, H. Simulating the Coupled Structural—Electronic Dynamics of Photo-Excited Lead Iodide Perovskites. *J. Phys. Chem. Lett.* **2020**, *11*, 4448–4455.
- (50) Hourahine, B.; Aradi, B.; Blum, V.; Bonafé, F.; Buccheri, A.; Camacho, C.; Cevallos, C.; Deshaye, M. Y.; Dumitrică, T.; Dominguez, A.; et al. DFTB+, a Software Package for Efficient Approximate Density Functional Theory Based Atomistic Simulations. *J. Chem. Phys.* **2020**, *152*, 124101.
- (51) Aradi, B.; Hourahine, B.; Frauenheim, Th DFTB+, a Sparse Matrix-Based Implementation of the DFTB Method. *J. Phys. Chem. A* **2007**, *111*, 5678–5684.
- (52) Bonafe, F. P.; et al. A Real-Time Time-Dependent Density Functional Tight-Binding Implementation for Semiclassical Excited State Electron—Nuclear Dynamics and Pump—Probe Spectroscopy Simulations. J. Chem. Theory Comput. 2020, 16, 4454—4469.
- (53) Malone, W.; Nebgen, B.; White, A.; Zhang, Y.; Song, H.; Bjorgaard, J. A.; Sifain, A. E.; Rodriguez-Hernandez, B.; Freixas, V. M.; Fernandez-Alberti, S.; et al. NEXMD Software Package for Non-Adiabatic Excited State Molecular Dynamics Simulations. *J. Chem. Theory Comput.* **2020**, *16*, 5771–5783.
- (54) Sifain, A. E.; Bjorgaard, J. A.; Nelson, T. R.; Nebgen, B. T.; White, A. J.; Gifford, B. J.; Gao, D. W.; Prezhdo, O. V.; Fernandez-Alberti, S.; Roitberg, A. E.; et al. Photoexcited Nonadiabatic

- Dynamics of Solvated Push–Pull π -Conjugated Oligomers with the NEXMD Software. *J. Chem. Theory Comput.* **2018**, 14, 3955–3966.
- (55) Tretiak, S.; Mukamel, S. Density Matrix Analysis and Simulation of Electronic Excitations in Conjugated and Aggregated Molecules. *Chem. Rev.* **2002**, *102*, 3171–3212.
- (56) Mukamel, S. Electronic Coherence and Collective Optical Excitations of Conjugated Molecules. *Science* **1997**, *277*, 781–787.
- (57) Shimojo, F.; Hattori, S.; Kalia, R. K.; Kunaseth, M.; Mou, W.; Nakano, A.; Nomura, K.; Ohmura, S.; Rajak, P.; Shimamura, K.; et al. A Divide-Conquer-Recombine Algorithmic Paradigm for Large Spatiotemporal Quantum Molecular Dynamics Simulations. *J. Chem. Phys.* **2014**, *140*, 18A529.
- (58) Miyamoto, Y.; Rubio, A. Application of the Real-Time Time-Dependent Density Functional Theory to Excited-State Dynamics of Molecules and 2D Materials. *J. Phys. Soc. Jpn.* **2018**, *87*, 041016.
- (59) Provorse, M. R.; Isborn, C. M. Electron Dynamics with Real-Time Time-Dependent Density Functional Theory. *Int. J. Quantum Chem.* **2016**, *116*, 739–749.
- (60) Liu, J.; Zhang, X.; Lu, G. Excitonic Effect Drives Ultrafast Dynamics in van Der Waals Heterostructures. *Nano Lett.* **2020**, 20, 4631–4637.
- (61) Wu, G.; Li, Z.; Zhang, X.; Lu, G. Charge Separation and Exciton Dynamics at Polymer/ZnO Interface from First-Principles Simulations. *J. Phys. Chem. Lett.* **2014**, *5*, 2649–2656.
- (62) Akimov, A. V. Libra: An Open-Source "Methodology Discovery" Library for Quantum and Classical Dynamics Simulations. *J. Comput. Chem.* **2016**, 37, 1626–1649.
- (63) Akimov, A. V.; Smith, B.; Shakiba, M.; Sato, K.; Temen, S.; Li, W.; Sun, X.; Chan, M. Quantum-Dynamics-Hub/Libra-Code: Hotfix for the TD-DFT/NAMD with Libra (Version 4.9.1); Zenodo, 2020-10-31. DOI: 10.5281/zenodo.4162542.
- (64) Kühne, T. D.; Iannuzzi, M.; Del Ben, M.; Rybkin, V. V.; Seewald, P.; Stein, F.; Laino, T.; Khaliullin, R. Z.; Schütt, O.; Schiffmann, F.; et al. CP2K: An Electronic Structure and Molecular Dynamics Software Package Quickstep: Efficient and Accurate Electronic Structure Calculations. J. Chem. Phys. 2020, 152, 194103.
- (65) Hutter, J.; Iannuzzi, M.; Schiffmann, F.; VandeVondele, J. CP2K: Atomistic Simulations of Condensed Matter Systems. *Wiley Interdiscip. Rev. Comput. Mol. Sci.* **2014**, *4*, 15–25.
- (66) Perdew, J. P.; Burke, K.; Ernzerhof, M. Generalized Gradient Approximation Made Simple. *Phys. Rev. Lett.* **1996**, *77*, 3865–3868.
- (67) Kümmel, S. Charge-Transfer Excitations: A Challenge for Time-Dependent Density Functional Theory That Has Been Met. *Adv. Energy Mater.* **2017**, *7*, 1700440.
- (68) Lin, Y.; Akimov, A. V. Dependence of Nonadiabatic Couplings with Kohn—Sham Orbitals on the Choice of Density Functional: Pure vs Hybrid. *J. Phys. Chem. A* **2016**, *120*, 9028—9041.
- (69) Cohen, A. J.; Mori-Sánchez, P.; Yang, W. Challenges for Density Functional Theory. *Chem. Rev.* **2012**, *112*, 289–320.
- (70) Autschbach, J. Charge-Transfer Excitations and Time-Dependent Density Functional Theory: Problems and Some Proposed Solutions. *ChemPhysChem* **2009**, *10*, 1757–1760.
- (71) Dreuw, A.; Weisman, J. L.; Head-Gordon, M. Long-Range Charge-Transfer Excited States in Time-Dependent Density Functional Theory Require Non-Local Exchange. *J. Chem. Phys.* **2003**, *119*, 2943–2946.
- (72) Hartwigsen, C.; Gøedecker, S.; Hutter, J. Relativistic Separable Dual-Space Gaussian Pseudopotentials from H to Rn. *Phys. Rev. B: Condens. Matter Mater. Phys.* **1998**, *58*, 3641.
- (73) VandeVondele, J.; Hutter, J. Gaussian Basis Sets for Accurate Calculations on Molecular Systems in Gas and Condensed Phases. *J. Chem. Phys.* **200**7, *127*, 114105.
- (74) Monkhorst, H. J.; Pack, J. D. Special Points for Brillouin-Zone Integrations. *Phys. Rev. B* **1976**, *13*, 5188–5192.
- (75) Grimme, S.; Antony, J.; Ehrlich, S.; Krieg, H. A Consistent and Accurate *Ab Initio* Parametrization of Density Functional Dispersion Correction (DFT-D) for the 94 Elements H-Pu. *J. Chem. Phys.* **2010**, 132, 154104.

- (76) Bussi, G.; Donadio, D.; Parrinello, M. Canonical Sampling through Velocity-Rescaling. *J. Chem. Phys.* **2007**, *126*, 014101.
- (77) Press, W. H.; Teukolsky, S. A.; Vetterling, W. T.; Flannery, B. P. *Numerical Recipes 3rd ed.: The Art of Scientific Computing*; Cambridge University Press: Cambridge, U.K., 2007.
- (78) Sutton, R. J.; Eperon, G. E.; Miranda, L.; Parrott, E. S.; Kamino, B. A.; Patel, J. B.; Hörantner, M. T.; Johnston, M. B.; Haghighirad, A. A.; Moore, D. T.; et al. Bandgap-Tunable Cesium Lead Halide Perovskites with High Thermal Stability for Efficient Solar Cells. *Adv. Energy Mater.* **2016**, *6*, 1502458.
- (79) Eperon, G. E.; Paternò, G. M.; Sutton, R. J.; Zampetti, A.; Haghighirad, A. A.; Cacialli, F.; Snaith, H. J. Inorganic Caesium Lead Iodide Perovskite Solar Cells. *J. Mater. Chem. A* **2015**, *3*, 19688–19695.
- (80) Chu, W.; Saidi, W. A.; Zhao, J.; Prezhdo, O. V. Soft Lattice and Defect Covalency Rationalize Tolerance of β -CsPbI₃ Perovskite Solar Cells to Native Defects. *Angew. Chem., Int. Ed.* **2020**, *59*, 6435–6441.
- (81) Zhou, L.; Neukirch, A. J.; Vogel, D. J.; Kilin, D. S.; Pedesseau, L.; Carignano, M. A.; Mohite, A. D.; Even, J.; Katan, C.; Tretiak, S. Density of States Broadening in CH₃NH₃PbI₃ Hybrid Perovskites Understood from Ab Initio Molecular Dynamics Simulations. *ACS Energy Lett.* **2018**, *3*, 787–793.
- (82) Akimov, A. V.; Prezhdo, O. V. The PYXAID Program for Non-Adiabatic Molecular Dynamics in Condensed Matter Systems. *J. Chem. Theory Comput.* **2013**, *9*, 4959–4972.
- (83) Akimov, A. V.; Prezhdo, O. V. Advanced Capabilities of the PYXAID Program: Integration Schemes, Decoherence Effects, Multiexcitonic States, and Field-Matter Interaction. *J. Chem. Theory Comput.* **2014**, *10*, 789–804.
- (84) Chen, Z.; Zhang, P.-Z.; Zhou, Y.; Zhang, X.; Liu, X.; Hou, Z.; Tang, J.; Li, W. Elucidating the Influence of Sulfur Vacancies on Nonradiative Recombination Dynamics in Cu₂ZnSnS₄ Solar Absorbers. *J. Phys. Chem. Lett.* **2020**, *11*, 10354–10361.
- (85) Li, W.; Chen, Z.; Tang, J.; Prezhdo, O. V. Anti-Correlation between Band Gap and Carrier Lifetime in Lead Halide Perovskites under Compression Rationalized by Ab Initio Quantum Dynamics. *Chem. Mater.* **2020**, 32, 4707–4715.
- (86) Niu, X.; Bai, X.; Zhou, Z.; Wang, J. Rational Design and Characterization of Direct Z-Scheme Photocatalyst for Overall Water Splitting from Excited State Dynamics Simulations. *ACS Catal.* **2020**, *10*, 1976–1983.
- (87) Zhang, L.; Chu, W.; Zheng, Q.; Benderskii, A. V.; Prezhdo, O. V.; Zhao, J. Suppression of Electron—Hole Recombination by Intrinsic Defects in 2D Monoelemental Material. *J. Phys. Chem. Lett.* **2019**, *10*, 6151–6158.
- (88) Xu, C.; Gu, F. L.; Zhu, C. Ultrafast Intersystem Crossing for Nitrophenols: Ab Initio Nonadiabatic Molecular Dynamics Simulation. *Phys. Chem. Chem. Phys.* **2018**, *20*, 5606–5616.
- (89) Liang, Y.; Li, J.; Jin, H.; Huang, B.; Dai, Y. Photoexcitation Dynamics in Janus-MoSSe/WSe₂ Heterobilayers: Ab Initio Time-Domain Study. *J. Phys. Chem. Lett.* **2018**, *9*, 2797–2802.
- (90) Li, W.; Tang, J.; Casanova, D.; Prezhdo, O. V. Time-Domain Ab Initio Analysis Rationalizes the Unusual Temperature Dependence of Charge Carrier Relaxation in Lead Halide Perovskite. *ACS Energy Lett.* **2018**, *3*, 2713–2720.
- (91) Wei, Y.; Zhou, Z.; Fang, W.-H.; Long, R. Grain Boundary Facilitates Photocatalytic Reaction in Rutile TiO₂ Despite Fast Charge Recombination: A Time-Domain *Ab Initio* Analysis. *J. Phys. Chem. Lett.* **2018**, *9*, 5884–5889.
- (92) Wiebeler, C.; Plasser, F.; Hedley, G. J.; Ruseckas, A.; Samuel, I. D. W.; Schumacher, S. Ultrafast Electronic Energy Transfer in an Orthogonal Molecular Dyad. *J. Phys. Chem. Lett.* **2017**, *8*, 1086–1092.
- (93) Zhou, X.; Li, L.; Dong, H.; Giri, A.; Hopkins, P. E.; Prezhdo, O. V. Temperature Dependence of Electron—Phonon Interactions in Gold Films Rationalized by Time-Domain Ab Initio Analysis. *J. Phys. Chem. C* 2017, 121, 17488—17497.
- (94) Yang, Z.; Surrente, A.; Galkowski, K.; Miyata, A.; Portugall, O.; Sutton, R. J.; Haghighirad, A. A.; Snaith, H. J.; Maude, D. K.; Plochocka, P.; et al. Impact of the Halide Cage on the Electronic

- Properties of Fully Inorganic Cesium Lead Halide Perovskites. ACS Energy Lett. 2017, 2, 1621–1627.
- (95) Miyata, A.; Mitioglu, A.; Plochocka, P.; Portugall, O.; Wang, J. T.-W.; Stranks, S. D.; Snaith, H. J.; Nicholas, R. J. Direct Measurement of the Exciton Binding Energy and Effective Masses for Charge Carriers in Organic–Inorganic Tri-Halide Perovskites. *Nat. Phys.* **2015**, *11*, 582–587.
- (96) İzmaylov, A. F.; Scuseria, G. E. Why Are Time-Dependent Density Functional Theory Excitations in Solids Equal to Band Structure Energy Gaps for Semilocal Functionals, and How Does Nonlocal Hartree—Fock-Type Exchange Introduce Excitonic Effects? *J. Chem. Phys.* **2008**, *129*, 034101.
- (97) Pradhan, E.; Sato, K.; Akimov, A. V. Non-Adiabatic Molecular Dynamics with ΔSCF Excited States. *J. Phys.: Condens. Matter* **2018**, 30, 484002.
- (98) Yang, Y.; Tokina, M. V.; Fang, W.-H.; Long, R.; Prezhdo, O. V. Influence of Tungsten Doping on Nonradiative Electron—Hole Recombination in Monolayer MoSe₂ with Se Vacancies. *J. Chem. Phys.* **2020**, *153*, 154701.
- (99) Ghosh, D.; Neukirch, A. J.; Tretiak, S. Optoelectronic Properties of Two-Dimensional Bromide Perovskites: Influences of Spacer Cations. *J. Phys. Chem. Lett.* **2020**, *11*, 2955–2964.
- (100) Tully, J. C. Molecular Dynamics with Electronic Transitions. J. Chem. Phys. 1990, 93, 1061–1071.
- (101) Belyaev, A. K.; Lebedev, O. V. Nonadiabatic Nuclear Dynamics of Atomic Collisions Based on Branching Classical Trajectories. *Phys. Rev. A: At., Mol., Opt. Phys.* **2011**, *84*, 014701.
- (102) Smith, B.; Akimov, A. V. Hot Electron Cooling in Silicon Nanoclusters via Landau—Zener Nonadiabatic Molecular Dynamics: Size Dependence and Role of Surface Termination. *J. Phys. Chem. Lett.* 2020, 11, 1456–1465.
- (103) Smith, B.; Akimov, A. V. A Comparative Analysis of Surface Hopping Acceptance and Decoherence Algorithms within the Neglect of Back-Reaction Approximation. *J. Chem. Phys.* **2019**, *151*, 124107.
- (104) Nelson, T.; Fernandez-Alberti, S.; Roitberg, A. E.; Tretiak, S. Nonadiabatic Excited-State Molecular Dynamics: Treatment of Electronic Decoherence. *J. Chem. Phys.* **2013**, *138*, 224111.
- (105) Granucci, G.; Persico, M. Critical Appraisal of the Fewest Switches Algorithm for Surface Hopping. *J. Chem. Phys.* **2007**, *126*, 134114.
- (106) Smith, B.; Shakiba, M.; Akimov, A. V. Nonadiabatic Dynamics in Si and CdSe Nanoclusters: Many-Body vs Single-Particle Treatment of Excited States. *J. Chem. Theory Comput.* **2021**, 17, 678–693.
- (107) Cui, P. Effect of Boron and Nitrogen Doping on Carrier Relaxation Dynamics of Graphene Quantum Dots. *Mater. Res. Express* **2018**, *5*, 065034.
- (108) Bretschneider, S. A.; Weickert, J.; Dorman, J. A.; Schmidt-Mende, L. Research Update: Physical and Electrical Characteristics of Lead Halide Perovskites for Solar Cell Applications. *APL Mater.* **2014**, 2, 040701.
- (109) Shen, Q.; Ripolles, T. S.; Even, J.; Zhang, Y.; Ding, C.; Liu, F.; Izuishi, T.; Nakazawa, N.; Toyoda, T.; Ogomi, Y.; et al. Ultrafast Selective Extraction of Hot Holes from Cesium Lead Iodide Perovskite Films. *J. Energy Chem.* **2018**, *27*, 1170–1174.
- (110) Shen, Q.; Ripolles, T. S.; Even, J.; Ogomi, Y.; Nishinaka, K.; Izuishi, T.; Nakazawa, N.; Zhang, Y.; Ding, C.; Liu, F.; et al. Slow Hot Carrier Cooling in Cesium Lead Iodide Perovskites. *Appl. Phys. Lett.* **2017**, *111*, 153903.
- (111) Li, W.; Zhou, L.; Prezhdo, O. V.; Akimov, A. V. Spin—Orbit Interactions Greatly Accelerate Nonradiative Dynamics in Lead Halide Perovskites. ACS Energy Lett. 2018, 3, 2159–2166.
- (112) Bernardi, M.; Vigil-Fowler, D.; Lischner, J.; Neaton, J. B.; Louie, S. G. Ab Initio Study of Hot Carriers in the First Picosecond after Sunlight Absorption in Silicon. *Phys. Rev. Lett.* **2014**, *112*, 257402.
- (113) Smith, B.; Shakiba, M. AkimovLab/Project_-CsPbI3 MB vs SP: Data Files for Nonadiabatic Dynamics Studies of

Excited States Dynamics in Cubic and Tetragonal CsPbI₃ (Version v1.0.0); Zenodo, 2020-12-18. DOI: 10.5281/zenodo.4358464.